Surface vibrations and (2×1) superstructures on fcc (110) metal surfaces

Joseph A. Stroscio, M. Persson,* and W. Ho
Laboratory of Atomic and Solid State Physics, and Materials Science Center, Cornell University, Ithaca, New York, 14853-2501
(Received 15 October 1985)

Electron-energy-loss spectra are presented for a number of adsorbate overlayers which form (2×1) superstructures on the fcc (110) surfaces of Ni and Cu. These include (2×1) structures of H, N_2, CO, and O. Lattice-dynamical slab calculations are used to analyze the vibrational properties observed in the loss spectra which result from symmetry selection rules for dipole activity of the surface phonons. The calculated spectral densities, together with the symmetry selection rules, are used to analyze proposed models for the adsorbate overlayer structures.

I. INTRODUCTION

The study of the vibrational properties of clean and adsorbate-covered surfaces is an area of fundamental interest in surface physics. In these studies, the application of electron-energy-loss spectroscopy (EELS) has been shown to be a powerful technique.[1] Information regarding the surface structure and interatomic forces may be obtained from an analysis of the vibrational spectra of the clean surface, while the adsorption-site symmetry and bond distances may be extracted from the vibrational modes of adsorbate-covered surfaces. Previous EELS studies of surface-phonon vibrations on clean and adsorbate-covered surfaces have focused mainly on the low-index fcc (100) and fcc (111) surfaces, such as the Ni(100),[2-6] Ni(111),[7] and Cu(100) surfaces.[3,5,8]

A complete description of the inelastic electron scattering from those surfaces requires an understanding of both the scattering process and the dynamics of the surface. Lattice-dynamical calculations for these systems have used a number of calculational schemes such as the Green's-function techniques,[9,10] continued-fraction method,[11] and finite slabs.[12-14] In the case of ordered adsorbate overlayers, direct information concerning the adsorption-site configuration may be obtained in some cases, from a simple symmetry analysis based on selection rules for dipole scattering.[5,15]

In this paper we discuss the analysis of the vibrational spectra of ordered overlayers on the fcc (110) surfaces of Ni and Cu, which were observed by inelastic dipole scattering. The fcc (110) surface vibrations have been less studied in comparison to the other two low-index surfaces. However, recent lattice-dynamical calculations[16] and experimental measurements[17] show a rich surface-phonon spectrum for this surface. In this paper we first present for completeness the relevant spectral function in the EELS cross section and its relation to the dipole-active displacements of the surface layers. The lattice-dynamical calculations employed here use the finite-slab method. This method was chosen for its simplicity and the ease in which changes in the surface structure may be accommodated. The particular systems analyzed are ordered adsorbate overlayers of H, N_2, CO, and O which exhibit (2×1) superstructures on the Ni(110) and Cu(110) surfaces. The tendency for adsorbates to form (2×1) structures on the fcc (110) surface results from the unique anisotropy of this surface. As shown in Fig. 1(a) this surface consists of closed packed rows separated by troughs along the $[1\bar{1}0]$ direction. In the case of oxygen adsorption on these surfaces, a reconstruction of the surface takes place.

Results for the (2×1)H structure are found to be consistent with the buckled-bridge geometry deduced from previous He-diffraction and low-energy electron-diffraction (LEED) results. For the (2×1)N_2 and (2×1)CO structures on the Ni and Cu surfaces, respectively, the spectral-density calculations are in agreement with a terminally bonded configuration. The spectra observed for the (2×1)CO structure are found to be consistent with a previously proposed tilting geometry of the CO molecule. For the (2×1)O structure the densities of states are presented for two different models of the surface reconstruction and are compared to the measured loss spectra from the Ni(110) and Cu(110) surfaces.

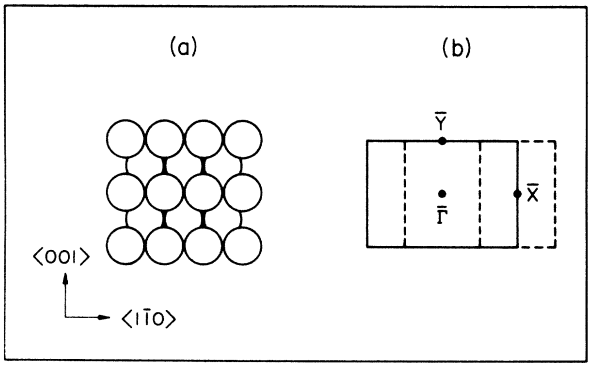

FIG. 1. Atomic arrangement of the fcc (110) surface and the corresponding surface Brillouin zone (SBZ). The dashed line shows the reduced SBZ for an adsorbate overlayer in a (2×1) configuration.

II. EXPERIMENTAL DETAILS

The experiments were performed in a multitechnique two-level ultrahigh-vacuum system which is described in detail elsewhere.[18] Briefly, the upper level contains facilities for sample cleaning, gas dosing, LEED or Auger-electron spectroscopy (AES), and thermal desorption spectroscopy (TDS). The lower level houses the electron-energy-loss spectrometer, which consists of a double-pass 127° electrostatic deflector for the monochromator and analyzer.[19] The scattering geometry is fixed with a total scattering angle of 120°. The scattering plane containing the incident and scattered electrons is defined by the surface normal and the $[1\bar{1}0]$ crystal direction. All spectra were recorded in the specular direction with an overall resolution of 5 meV (40 cm^{-1}) full-width at half-maximum (FWHM). The electron-impact energies, referenced to the clean surfaces, were 3.2 and 4.3 eV for Cu and Ni, respectively.

The samples consisted of circular disks 1 cm in diameter and 2 mm thick. They were spot-welded between two 0.5-mm-diam wires to a low-temperature mainipulator.[20] Ta wire was used for the Ni sample while Pt wire gave a secure spotweld for the Cu sample. Sample cleaning consisted of neon-ion bombardment (500 eV) and annealing to 750 and 1050 K for Cu and Ni, respectively. The sample was heated resistively and its temperature was monitored by a Chromel-Alumel thermocouple which was spot-welded to the back of the Ni sample and placed in physical contact with the edge of the Cu crystal.

Research-grade H_2, N_2, CO, and O_2 (Matheson) were used for gas dosing. Ordered (2×1) overlayers were produced by monitoring the low-energy electron-diffraction pattern during exposure until a sharp well-ordered (2×1) pattern was observed. The LEED apparatus employed here is a custom-made unit consisting of a set of four-grid LEED optics incorporating two microchannel plates for image intensification. Due to the high gain of the microchannel plates, adverse electron-beam effects are virtually eliminated by using very low beam-current densities ($\sim 10^{-10}$ A cm^{-2}).

III. INELASTIC DIPOLE SCATTERING FROM SURFACE VIBRATIONS

The inelastic scattering of low-energy electrons from surfaces can be described by two scattering mechanisms which can be conveniently discerned by the appropriate scattering geometry.[21] These are dipole scattering from the long-range Coulomb interactions between the incident electron and the electric field fluctuations associated with the surface modes, and impact scattering from short-range interactions with the atomic potentials of the surface atoms. Dipole scattering is associated with an intensity distribution which peaks sharply in the specular direction, corresponding to very small wave-vector transfer parallel to the surface, $\mathbf{Q}_{\parallel}\approx 0$.[1] In contrast, impact scattering is typically associated with a broad angular distribution and gives a small contribution in the specular direction in comparison to dipole-excited modes.[21]

The theory of dipole scattering from surfaces is well established.[1,22,23] The inelastic cross section obtained in the Born approximation is given by a product of two factors. The first is a kinematic factor which depends on the scattering geometry and is independent of the properties of the substrate. The second factor is related to the correlation function of the charge-density fluctuations in the surface region.[23] In the application to vibrational motion, this factor is the spectral function $S(\omega)$ for the dipole-dipole correlation function which is defined as

$$S(\omega)=\frac{1}{N}\int \frac{dt}{2\pi} e^{i\omega t}\langle \mu_z(t)\mu_z(0)\rangle \ , \tag{1}$$

where μ_z is the normal component of the total dynamic dipole moment, N is the number of surface primitive cells, and the angular brackets denote a statistical average.

The semi-infinite crystal may be regarded as a system of planes of nuclei, with each plane parallel to the surface. Let the position of each atom be denoted by $\mathbf{R}(\mathbf{L},k)$, where $\mathbf{L}=(\mathbf{L}_{\parallel},L_z)$, $\mathbf{L}_{\parallel}$ is a vector parallel to the surface directed to a particular unit cell, L_z denotes a particular atomic layer, and the index k specifies the different atoms within the unit cell. The relation between the normal component of the total dipole moment and the displacement $\mathbf{u}(\mathbf{L},k)$ of an atom away from equilibrium is given by the effective charge field $\mathbf{e}^*(\mathbf{L},k)$ defined by

$$\mu_z=\sum_{\mathbf{L},k}\mathbf{e}^*(\mathbf{L},k)\cdot\mathbf{u}(\mathbf{L},k) \ . \tag{2}$$

Due to the translational symmetry of the lattice we have $\mathbf{e}^*(\mathbf{L},k)=\mathbf{e}^*(L_z,k)$. Thus only displacement fields at the $\bar{\Gamma}$ point $\mathbf{Q}_{\parallel}=\mathbf{0}$ can give rise to a nonzero dipole moment μ_z.

The evaluation of the spectral function $S(\omega)$ thus involves determining a displacement-displacement correlation function. In the harmonic approximation the function $S(\omega)$ may be evaluated by expanding the displacement field $\mathbf{u}$ in terms of the eigenstates of the dynamical matrix $\vec{\mathbf{D}}$ as[24]

$$\mathbf{u}(\mathbf{Q}_{\parallel}=\mathbf{0};L_z,k;t)=\left[\frac{\hbar N}{2M(L_z,k)}\right]^{1/2}\times\sum_{\lambda}\frac{\xi_{\lambda}(\mathbf{Q}_{\parallel}=\mathbf{0};L_z,k)}{\omega_{\lambda}^{1/2}}\times(a_{\lambda}^{\dagger}e^{i\omega_{\lambda}t}+a_{\lambda}e^{-i\omega_{\lambda}t}) \ , \tag{3}$$

where $a_{\lambda}^{\dagger}$ and a_{λ} are the phonon creation and annihilation operators which obey the commutation relations $[a_{\lambda},a_{\lambda'}^{\dagger}]=\delta_{\lambda\lambda'}$, and $M(L_z,k)$ is the mass of the kth atom in the L_zth layer. The eigenvectors ξ_{λ} are determined by the eigenvalue equation given by

$$\omega_{\lambda}^2\xi_{\lambda}(\mathbf{Q}_{\parallel};L_z,k)=\sum_{L_z',k'}\vec{\mathbf{D}}(\mathbf{Q}_{\parallel};L_z,k;L_z',k')\xi_{\lambda}(\mathbf{Q}_{\parallel};L_z',k') \ , \tag{4}$$

where eigenvectors ξ_{λ} obey the usual orthonormality and closure relations. The matrix $\vec{\mathbf{D}}$ is the Fourier-transformed dynamical matrix given by

$$\overleftrightarrow{D}(\vec{Q}_{||};L_z,k;L_z',k') = \sum_{L_{||}} \frac{\overleftrightarrow{\Phi}(\mathbf{L},k;\mathbf{L}',k')}{[M(L_z,k)M(L_z',k')]^{1/2}} \times \exp\{-i\mathbf{Q}_{||}\cdot[\mathbf{R}(\mathbf{L},k)-\mathbf{R}(\mathbf{L}',k')]\} , \quad (5)$$

where $\overleftrightarrow{\Phi}$ is the force-constant matrix.[25]

With the use of Eqs. (2) and (3) the spectral function $S(\omega)$ can be directly related to a phonon density of states, $g(\omega,[\mathbf{v}^*(L_z,k)])$, projected onto a normalized effective charge field $\mathbf{v}^*(L_z,k)$ as

$$S(\omega)=\frac{\hbar(e^*_{\rm tot})^2}{2M^*\omega}[1+n(\omega)]g(\omega,[\mathbf{v}^*(L_z,k)]) , \quad (6)$$

where

$$\mathbf{v}^*(L_z,k)=\frac{(M^*)^{1/2}}{e^*_{\rm tot}}\frac{\mathbf{e}^*(L_z,k)}{[M(L_z,k)]^{1/2}} , \quad (7)$$

$$e^*_{\rm tot}=\left[\sum_{L_z,k}\mathbf{e}^*(L_z,k)^2\right]^{1/2} , \quad (8)$$

$$M^*=\frac{(e^*_{\rm tot})^2}{\sum_{L_z,k}\mathbf{e}^*(L_z,k)^2/M(L_z,k)} , \quad (9)$$

and

$$g(\omega,[\mathbf{v}^*(L_z,k)]) = \sum_{\lambda}\left|\sum_{L_z,k}\xi_\lambda(L_z,k)\cdot\mathbf{v}^*(L_z,k)\right|^2\delta(\omega-\omega_\lambda) . \quad (10)$$

Here $n(\omega)$ is the Bose-Einstein distribution factor, $e^*_{\rm tot}$ is the magnitude of the effective charge field, and M^* is the effective mass of the dipole-active field.

The evaluation of the spectral function is facilitated by considering the symmetry of the system. Due to symmetry, the dynamical matrix factors so that displacement fields belonging to different symmetry classes are decoupled. Furthermore, the dipole selection rule states that only the totally symmetric displacement fields at the $\bar{\Gamma}$ point of the surface Brillouin zone (SBZ) are dipole active. This selection rule follows simply from the invariance of the total dynamic dipole moment for all operations belonging to the symmetry group for the system.[10] Thus for the evaluation of the spectral function it is necessary only to consider those displacement fields which are totally symmetric at the $\bar{\Gamma}$ point of the SBZ. The H and CO adsorbate structures discussed in Sec. V have a glide-line symmetry and the more general formulation of the dipole selection rule is needed; only totally symmetric displacement fields with respect to the full symmetry group are dipole active.

In the modeling of the effective charge field we make the assumption that the effective charges $\mathbf{e}^*(L_z,k)$ are nonzero only for the adsorbate layer and the outermost substrate layer. This assumption is based on the fact that the efficient screening by the conduction electrons will limit the dipole activity to the outermost surface layers. Additionally, it has been shown that the dipole activity should be modeled by the bond-stretch displacements between the adsorbate and the substrate atoms when a detailed comparison of intensities between theory and experiment is required.[26]

To calculate the vibrational projected density of states given by Eq. (10) we use the finite-slab method for the phonon dynamics. This involves the diagonalization of the dynamical matrix in Eq. (5) for a finite number of atomic layers. The corresponding density of states constructed from Eq. (10) by projecting the eigenmodes on the dipole-active displacement field will then consist of a discrete set of peaks located at the eigenfrequencies. The limited energy resolution in measured energy-loss spectra is described by replacing these peaks by a normalized Gaussian distribution with a width given by the experimental resolution. For a typical energy resolution of 5 meV such a calculated spectrum is found to be converged with slabs having as little as 25 layers. Finer details in the phonon spectrum may be resolved with thicker slabs, with 100 atomic layers easily accommodated with present-day computers. The size of the matrix to be diagonalized, and hence the computation time, can be significantly reduced by considering only those displacement fields which are symmetry allowed, according to the dipole selection rule, and which may be decoupled in the dynamical matrix.

IV. THE BARE SURFACE

A necessary ingredient in the lattice-dynamical calculations for the bare surface is a proper description of the interatomic forces. For Cu and Ni substrates an accurate description is achieved by a nearest-neighbor central-force-constant model for the phonon dynamics.[16,27] In this model there is only one parameter, the maximum bulk-phonon frequency Ω_b, which is adjusted to fit the measured bulk-phonon spectra. For Cu and Ni, Ω_b is equal to 29.7 and 36.7 meV, respectively. More sophisticated models of the phonon dynamics for Cu and Ni exist which account for second-neighbor and angle-bending interactions.[28] Incorporation of these extra terms in the phonon dynamics only affected the surface-mode frequencies a few percent. This results from the fact that the angle-bending and second-neighbor force constants are $\lesssim 10\%$ of the nearest-neighbor force constant. Thus the single-parameter nearest-neighbor central-force-constant model is adopted in our calculations for its accuracy and simplicity.

In modeling the surface force constants, we use the truncated crystal approximation, where the loss of coordination of the surface atoms is the only effect considered in determining the surface force constants. Thus the surface force constants are determined uniquely by the bulk values. This approximation was shown to be adequate in describing previous experimental results on the clean Ni(110) and Cu(110) surfaces.[16,17] Recent measurements of surface-phonon dispersions on Ni(100), along with lattice-dynamical calculations, have concluded a 20% increase in the surface interlayer force constant with a 1.7–3.3% contraction of the top layer.[2] Our previous re-

sults indicate that such a large change in the surface force constants is not present on the Ni(110) or Cu(110) surfaces and that the surface force constants can be modeled after the bulk values within an accuracy of ±15%.

Using the nearest-neighbor central-force-constant model, the evaluation of the dynamical matrix in Eq. (5) for the fcc (110) surface is straightforward. The force-constant matrix is given by

$$\Phi_{\alpha\beta}(\mathbf{L},\mathbf{L}')=-\phi''(a_0)\hat{\mathbf{n}}_\alpha(\mathbf{L},\mathbf{L}')\hat{\mathbf{n}}_\beta(\mathbf{L},\mathbf{L}') +\delta_{\mathbf{L},\mathbf{L}'}\sum_{\mathbf{L}''}\phi''(a_0)\hat{\mathbf{n}}_\alpha(\mathbf{L},\mathbf{L}'')\hat{\mathbf{n}}_\beta(\mathbf{L},\mathbf{L}''), \quad (11)$$

where in a description based on pairwise central potentials $\phi''(a_0)$ is the second derivative of the two-body interaction between atoms L and L′ evaluated at their equilibrium position a_0 and when $\mathbf{L}\neq\mathbf{L}'$ are nearest neighbors,

$$\hat{\mathbf{n}}_\alpha(\mathbf{L},\mathbf{L}')=[\mathbf{R}(\mathbf{L}')-\mathbf{R}(\mathbf{L})]_\alpha/|\mathbf{R}(L')-\mathbf{R}(L)|, \quad (12)$$

and zero otherwise. With nearest-neighbor central forces $\phi''(a_0)$ is related to the maximum bulk-phonon frequency as $\phi''(a_0)/M_s=\Omega_b^2/8$, where M_s is the mass of a substrate atom.

With the force-constant matrices defined above, we consider a finite slab with atomic planes parallel to the (110) surface. Then the only nonzero matrices $\overleftrightarrow{\mathbf{D}}_{\alpha\beta}(\mathbf{Q}_{||};L_z,L_z')$ defined in Eq. (5) are those with $L_z=L_z'\pm1,\pm2$. With $d_{\alpha\beta}=D_{\alpha\beta}/\Omega_b^2$, $q_x=Q_x a_0/\pi$, and $q_y=Q_y a_0\sqrt{2}/\pi$, we have for the bulk matrices,

$$d(\mathbf{Q}_{||};L_z,L_z)=\frac{1}{4}\begin{bmatrix}2-\cos(\pi q_x) & 0 & 0\\ 0 & 2 & 0\\ 0 & 0 & 2\end{bmatrix}, \quad (13a)$$

$$d(\mathbf{Q}_{||};L_z,L_z+1)=-\frac{1}{8}\begin{bmatrix}\cos(\pi q_x/2)\cos(\pi q_y/2) & -\sqrt{2}\sin(\pi q_x/2)\sin(\pi q_y/2) & i\sin(\pi q_x/2)\sin(\pi q_y/2)\\ -\sqrt{2}\sin(\pi q_x/2)\sin(\pi q_y/2) & 2\cos(\pi q_x/2)\cos(\pi q_y/2) & -i\sqrt{2}\cos(\pi q_y/2)\sin(\pi q_y/2)\\ i\sin(\pi q_x/2)\cos(\pi q_y/2) & -i\sqrt{2}\cos(\pi q_x/2)\sin(\pi q_y/2) & \cos(\pi q_x/2)\cos(\pi q_y/2)\end{bmatrix}, \quad (13b)$$

$$d(\mathbf{Q}_{||};L_z,L_z-1)=d^*(\mathbf{Q}_{||};L_z,L_z+1), \quad (13c)$$

$$d(\mathbf{Q}_{||};L_z,L_z\pm2)=-\frac{1}{8}\begin{bmatrix}0 & 0 & 0\\ 0 & 0 & 0\\ 0 & 0 & 1\end{bmatrix}. \quad (13d)$$

We obtain the surface matrices in a similar way using a truncated crystal, where the loss in coordination of the surface atoms is the only effect considered. These matrices are given by

$$d(\mathbf{Q}_{||};1,1)=\frac{1}{4}\begin{bmatrix}\frac{3}{2}-\cos(\pi q_x) & 0 & 0\\ 0 & 1 & 0\\ 0 & 0 & 1\end{bmatrix}, \quad (14a)$$

$$d(\mathbf{Q}_{||};1,2)=d(\mathbf{Q}_{||};L_z,L_z+1), \quad (14b)$$

$$d(\mathbf{Q}_{||};1,3)=d(\mathbf{Q}_{||};L_z,L_z+2), \quad (14c)$$

$$d(\mathbf{Q}_{||};2,2)=\frac{1}{4}\begin{bmatrix}2-\cos(\pi q_x) & 0 & 0\\ 0 & 2 & 0\\ 0 & 0 & \frac{3}{2}\end{bmatrix}. \quad (14d)$$

The surface eigenmodes and eigenvectors for the finite slab with r atomic layers is then obtained by constructing the $3r\times3r$ dynamical matrix in Eq. (5) from the 3×3 submatrices given in Eqs. (13) and (14). Once the dynamical matrix is formed, standard algorithms are used to solve for the eigenvalues and eigenvectors.

In considering the effects of the substrate vibrations on the vibrational modes of adsorbate-covered surfaces, one is interested in the density of states projected on the surface layer for the totally symmetric displacement fields at those high-symmetry points in the substrate SBZ which are equivalent to the $\bar{\Gamma}$ point in the SBZ. For the (2×1) superstructures on the fcc (110) surface, it is the $\bar{\Gamma}$ and $\bar{X}$ points of the substrate SBZ which are equivalent to the $\bar{\Gamma}$ point of the overlayer SBZ, as shown in Fig. 1(b). Thus, depending on the adsorption-site symmetry, various surface vibrations at the $\bar{\Gamma}$ and $\bar{X}$ points may become dipole active by coupling to the motion of the adsorbate overlayer. The vibrational density of states projected on the motion of the outer surface layer is then obtained using the eigenmodes and eigenvectors obtained from diagonalizing the dynamical matrix for a finite slab at a particular value of $\mathbf{Q}_{||}$ as described above.

The density of states projected on the perpendicular motion of the Ni surface layer for the displacement field at the $\bar{\Gamma}$ point is shown in Fig. 2. The spectral intensity shows a resonance with a maximum at 23 meV for the perpendicular motion of the outer surface layer. This particular resonance at the $\bar{\Gamma}$ point is dipole active in the absence of an adsorbate overlayer and has been observed in our previous measurements of the clean surface.[17] Previous surface lattice-dynamical calculations show that the resonance results from a split-off state in a pseudo-band-gap resulting from the nonmonotonic longitudinal-bulk-phonon dispersion along the [110] direction. The results obtained from the finite-slab calculation, shown in Fig. 2, are in agreement with results obtained from more ela-

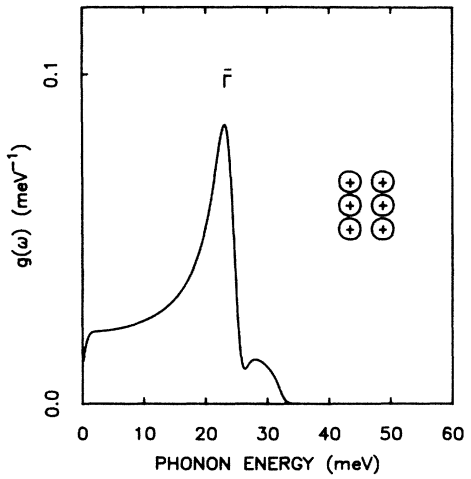

FIG. 2. Calculated vibrational density of states for the perpendicular motion of the outermost surface layer at the $\bar{\Gamma}$ point for the clean Ni surface. The peak at 23 meV corresponds to a vibrational resonance of the outermost surface layers (Refs. 16 and 17). The calculation used a 130-layer slab with 1 meV Gaussian broadening.

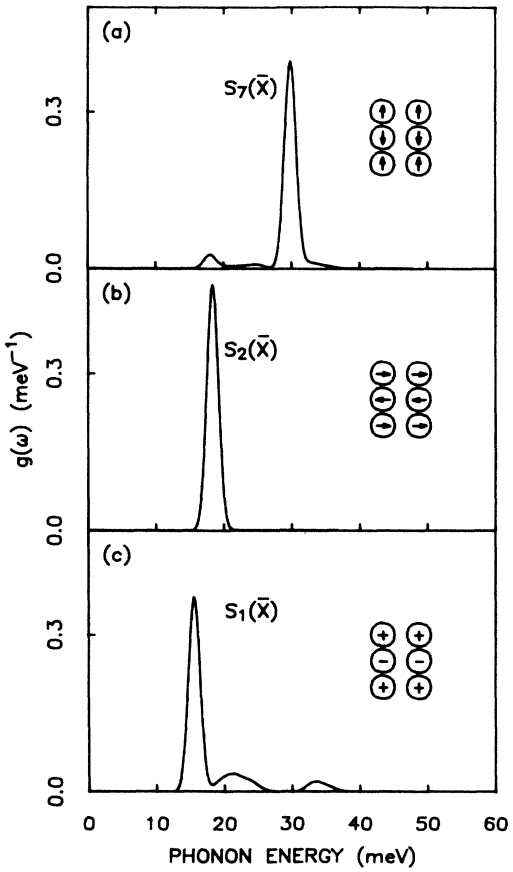

FIG. 3. Calculated vibrational density of states for the clean Ni surface at the $\bar{X}$ point in the substrate SBZ. (a)–(c) Projections on the motion of the outermost layer corresponding to the depicted displacement fields at $\bar{X}$. The sharp peaks correspond to the surface phonons $S_1(\bar{X})$, $S_2(\bar{X})$, and $S_7(\bar{X})$, according to the notation in Ref. 29. The calculations were performed on a 40-layer slab with 2 meV Gaussian broadening.

borate Green's-function calculations.[16]

The projected densities of states at the $\bar{X}$ point in the substrate SBZ are shown in Fig. 3 for the different displacement fields which are displayed. Along the $\bar{\Gamma}$–$\bar{X}$ direction the modes split into two classes resulting from the mirror-plane symmetry. The odd modes are polarized in the y direction and are decoupled in the dynamical matrix as seen in Eqs. (13) and (14). Similarly, the modes with x-z polarization are decoupled and can be considered separately in the lattice-dynamical calculations. The sharp peaks observed at 15.5, 18.4, and 29.8 meV correspond to the $S_1(\bar{X})$, $S_2(\bar{X})$, and $S_7(\bar{X})$ surface phonons observed in earlier surface lattice-dynamical calculations.[29] Also shown in the spectral densities for the surface layer are the contributions from the bulk subbands. The $S_1(\bar{X})$ surface phonon is the low-lying Rayleigh phonon, split off from the lower transverse bulk subband, and is polarized in the z direction. $S_2(\bar{X})$ is split off from the upper transverse bulk subband and is polarized in the y direction. Similarly, $S_7(\bar{X})$ is split off from the longitudinal bulk subband and is polarized in the x direction. The general behavior for surface modes to be split off from bulk subbands results from the lower restoring forces for the surface atoms due to the loss in coordination.

V. ADSORBATE OVERLAYERS WITH (2×1) SUPERSTRUCTURES

The degree of influence of the adsorbate on the spectral densities for the surface vibrations depends both on the adsorption site and the perturbation in the elements of the dynamical matrix describing the substrate. In analyzing the various (2×1) superstructures the displacement fields at the $\bar{\Gamma}$ and $\bar{X}$ points, shown in Figs. 2 and 3, are analyzed according to the adsorption-site symmetry. The effect of this symmetry on the vibrational density of states is illustrated, in particular, for the (2×1)N_2 overlayer on Ni(110). In the case of oxygen adsorption on these surfaces, the density of states is calculated for two different models of the surface reconstruction.

A. (2×1)H-Ni(110)

The interaction of hydrogen with Ni(110) has been a subject of many recent investigations due to the variety of ordered structures which form, depending on the H coverage and sample temperature. At low temperatures below ~180 K, LEED (Ref. 30) and He-diffraction (Ref. 31) measurements have shown that for coverages below one monolayer (ML), a sequence of H lattice-gas structures exist. In particular, a (2×1)-ordered hydrogen phase occurs at $\Theta=1$ ML. Results from He-diffraction measurements, which are consistent with LEED observations, suggest that the hydrogen atoms are located in a buckled-bridge geometry with the H atoms shifted off the short-bridge site toward the (111) microfacets as shown in Fig. 4(a). The unit cell for this structure contains two H atoms and possesses glide lines parallel to the [1$\bar{1}$0] direction. The glide-line symmetry results in the absence of $(n/2, 0)$, with n odd, diffraction spots in the LEED pattern observed at normal incidence.

Figure 4(b) shows the vibrational spectrum of the

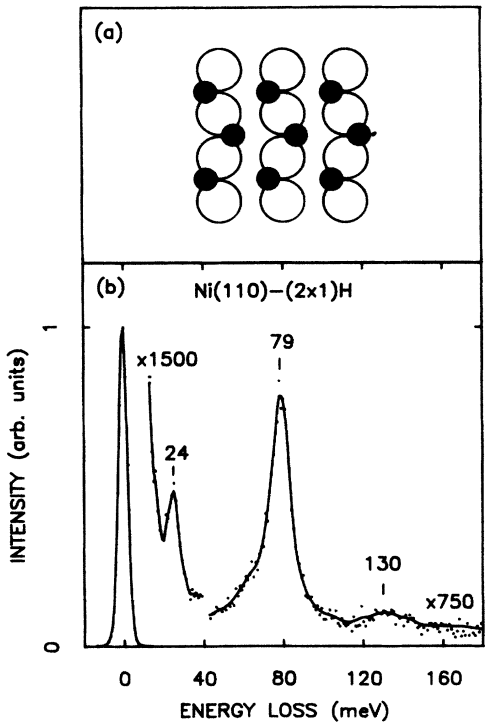

FIG. 4. (a) Model for the (2×1)H structure on Ni(110). The smaller solid circles represent hydrogen atoms. (b) Electron-energy-loss spectrum for the (2×1)H overlayer on Ni(110) at 80 K.

(2×1)H surface. Two losses are observed above the maximum bulk-phonon frequency at 79 and 130 meV which are in agreement with previous EELS measurements.[32] Based on recent calculations[33] these vibrational modes may be ascribed to the symmetric in-plane bending and stretching modes, respectively, of the H atoms in the pseudo-short-bridge sites as shown in Fig. 4(a).[34] The third loss feature at 24 meV lies below the maximum bulk-phonon frequency, which suggests that it is related to a surface mode at either the $\bar{\Gamma}$ or $\bar{X}$ points in the substrate SBZ.

A comparison with the spectral densities in Figs. 2 and 3 for the $\bar{\Gamma}$ and $\bar{X}$ points supports the interpretation of the observed loss feature at 24 meV in terms of the excitation of the surface-resonance mode at the $\bar{\Gamma}$ point in the substrate SBZ. The measured loss intensity of this surface-resonance mode agrees well with the observed loss intensity of this mode for the bare surface. In this situation the dipole activity of this mode is not introduced by the presence of the adsorbed H overlayer.

A consideration of the symmetry properties of the surface phonons at the $\bar{X}$ point indicates that all three modes, $S_1(\bar{X})$, $S_2(\bar{X})$, and $S_7(\bar{X})$, are symmetry forbidden for the adsorption-site configuration in Fig. 4(a). $S_1(\bar{X})$ and $S_7(\bar{X})$, for example, are odd under the glide-symmetry operation along the $[1\bar{1}0]$ direction, whereas $S_2(\bar{X})$ is odd under reflection symmetry through a plane parallel to the $(1\bar{1}0)$ plane. Only the symmetric vibration at the $\bar{\Gamma}$ point shown in Fig. 2 is symmetry allowed to be dipole active. Thus the observation of only one surface mode in the vibrational spectrum is consistent with the adsorption-site configuration in Fig. 4(a) as deduced from He-diffraction and LEED measurements.

B. (2×1)N_2-Ni(110)

The absorption of N_2 on Ni(110) represents an interesting chemisorption system where both commensurate and incommensurate overlayer structures are formed.[35] Unlike CO adsorption on this surface, however, N_2 on Ni(110) displays only a single N-N stretching vibration as a function of coverage.[36] CO on Ni(110), for example, displays three different C-O vibrational frequencies corresponding to different adsorption sites.[37] The fact that only a single N-N vibrational frequency is observed for the incommensurate phase for $\Theta \gtrsim 0.6$ ML,[35] where multiple sites are expected to be occupied, raises the question as

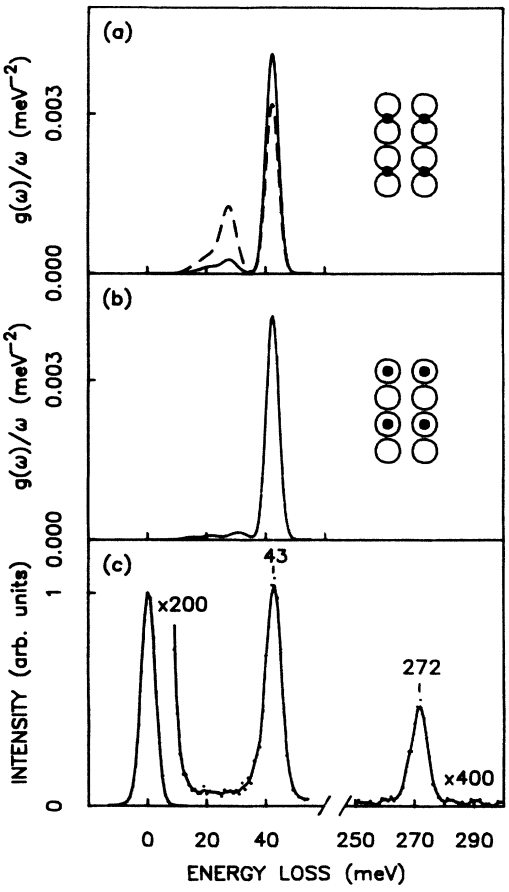

FIG. 5. Comparison between results from lattice-dynamical calculations and the experimental loss spectrum for the (2×1)-ordered overlayer on Ni(110). (a) Spectral density for the short-bridge adsorption-site configuration for two different dipole projections; a (solid line) projection on the bond-stretch displacements, and a (dashed line) projection on the surface-normal displacements. (b) Spectral density for the on-top adsorption-site configuration. (c) Experimental loss spectrum for the Ni(110)-(2×1)N_2 overlayer at 80 K. Note the break in the energy scale to display the N-N stretching vibration at 272 meV.

to whether the N-N stretching vibration can be used to discriminate between different adsorption sites.[36]

The vibrational spectra for the $(2\times1)N_2$ surface, corresponding to an N_2 coverage of 0.5 ML, is shown in Fig. 5(c). The N-N stretching vibration is observed at 272 meV while the N-Ni vibration is observed at 43 meV. These values are in agreement with previous EELS (Refs. 36 and 38) and ir (Ref. 39) measurements. Based on a comparison of the N-N stretching vibration with infrared spectra of inorganic complexes, a linearly bonded N_2 configuration was concluded.[38] The improved resolution in the spectra shown in Fig. 5(c) allows a comparison with lattice-dynamical calculations for various adsorption sites to be made in the spectral range below the maximum bulk-phonon frequency. Based on these calculations, an on-top adsorption-site configuration is confirmed for the $(2\times1)N_2$ structure.

In analyzing the $(2\times1)N_2$ structure, the density of states is calculated for both the on-top and short-bridge configurations for the adsorption site. A hard-sphere model is used to obtain the bond angles, taking the covalent radii of the nitrogen and nickel atoms as 0.75 and 1.25 Å, respectively. The nitrogen-nickel force constant ϕ_0'' is then adjusted to give agreement with the measured N-Ni vibrational frequency at 43 meV.

For the short-bridge-site configuration the substrate modes which are symmetry allowed to be dipole active are the displacement fields which correspond to the $S_7(\bar{X})$ surface phonon and the surface-resonance mode at $\bar{\Gamma}$. The density of states is obtained as described previously by constructing the dynamical matrix for a finite slab. The unit cell now contains two atoms per cell for the substrate due to the larger unit cell defined by the nitrogen overlayer. The submatrices in Eq. (13) are then 6×6 instead of 3×3. Due to the point-group symmetry of the short-bridge site, the displacement fields with y polarization are decoupled in the dynamical matrix. This reduces the size of the submatrices which need to be considered to 4×4. The resulting matrices for the surface layer at $\mathbf{Q}_{\parallel}=\mathbf{0}$ are

$$d(0,0)=\frac{2\phi_0''}{M_A\Omega_b^2}\begin{bmatrix}\cos^2\theta & 0 & 0 & 0\\ 0 & 0 & 0 & 0\\ 0 & 0 & \sin^2\theta & 0\\ 0 & 0 & 0 & 0\end{bmatrix}, \tag{15a}$$

$$d(0,1)=\frac{\phi_0''}{\Omega_b^2(M_AM_s)^{1/2}}\begin{bmatrix}-\cos^2\theta & -\cos^2\theta & -\sin\theta\cos\theta & \sin\theta\cos\theta\\ 0 & 0 & 0 & 0\\ -\sin\theta\cos\theta & \sin\theta\cos\theta & -\sin^2\theta & -\sin^2\theta\\ 0 & 0 & 0 & 0\end{bmatrix}, \tag{15b}$$

$$\Delta d(1,1)=\frac{\phi_0''}{\Omega_b^2M_s}\begin{bmatrix}\cos^2\theta & 0 & \sin\theta\cos\theta & 0\\ 0 & \cos^2\theta & 0 & -\sin\theta\cos\theta\\ \sin\theta\cos\theta & 0 & \sin^2\theta & 0\\ 0 & -\sin\theta\cos\theta & 0 & \sin^2\theta\end{bmatrix}, \tag{15c}$$

where $d(0,0)$ represents the adsorbate layer and M_s and M_A are the substrate and adsorbate masses, respectively. θ is the bond angle between the line joining the two bonding substrate atoms and the line joining the substrate and adsorbate atoms. Δd is the perturbation of the dynamical matrix, $\Delta d=d-d_0$, where d_0 is the unperturbed dynamical matrix of the substrate.

A detailed comparison of the relative intensities in the density of states with the measured EELS spectra is dependent on the projection for the dipole-active field. Previous analysis of EELS data for some adsorbate structures suggest that the dipole activity is mainly due to bond-stretch displacements between the adsorbate and the substrate atoms.[26] For the short-bridge site the normalized effective charge field can be expressed in terms of the angle δ as

$$\sum_{L_z,k}\xi_\lambda(L_z,k)\cdot\mathbf{V}^*(L_z,k)=\left[\frac{2\cos(\delta)\xi_{\lambda,z}(0,1)}{M_A^{1/2}}-\frac{\cos(\delta)\xi_{\lambda,z}(1,1)}{M_s^{1/2}}-\frac{\cos(\delta)\xi_{\lambda,z}(1,2)}{M_s^{1/2}}-\frac{\sin(\delta)\xi_{\lambda,x}(1,1)}{M_s^{1/2}}+\frac{\sin(\delta)\xi_{\lambda,x}(1,2)}{M_s^{1/2}}\right]\Big/\left[\frac{4\cos^2\delta}{M_A}+\frac{2}{M_s}\right]^{1/2}, \tag{16}$$

where δ is the angle between the dipole-active displacement of the substrate atom and the surface normal.

The vibrational density of states is shown in Fig. 5(a) for the two extreme cases $\delta=0°$ (dashed line) and $\delta=36.9°$ (solid line). $\delta=0°$ corresponds to displacements normal to the surface, whereas $\delta=36.9°$ corresponds to bond-stretch displacements. As observed in previous calculations,[26] the normal displacements tend to assign too large

an intensity in the bulk-phonon band, and a value of δ closer to bond-stretch displacements is more likely. The lower intensity of modes within the energy range of the bulk-phonon band, when the dipole-active displacements correspond to bond-stretch displacements rather than surface-normal displacements, can be understood from the following argument. For the modes in the energy range of the bulk-phonon band, the motion of the high-energy adsorbate mode follows almost instantaneously the motion of the substrate atoms in such a way that the bond distance is almost fixed. This results from the fact that the mass-weighted displacement field corresponding to bond-stretch displacements has almost the dominating dynamical matrix element. Thus a relative projection along the bond-stretch displacements gives a smaller contribution from the surface vibrations. This effect is increasingly more pronounced for modes with lower energy.

As predicted by the symmetry selection rules, $S_7(\bar{X})$ is observed to be dipole active with an appreciable intensity for the short-bridge-site configuration. Its frequency is slightly shifted from 29.8 meV for the bare surface to 27.8 meV for the nitrogen-covered surface. The $\bar{\Gamma}$ resonance is not resolved from the $S_7(\bar{X})$ surface phonon due to the finite broadening used in the calculation. A comparison of the experimental loss spectrum with the calculated density of states can then be used to rule out the short-bridge configuration for the adsorption site since there is no feature observed at 28 meV in the measured loss spectrum where $S_7(\bar{X})$ is expected.

For the on-top site configuration, the symmetry selection rules indicate that the displacements fields corresponding to the $S_1(\bar{X})$ surface phonon and the surface-resonance mode at $\bar{\Gamma}$ should be dipole active. Based on a symmetry analysis alone, an incorrect conclusion could be deduced by analyzing the measured spectra where no sharp features are observed below the maximum bulk-phonon frequency. A lattice-dynamical calculation is then necessary to obtain both the observed frequencies and intensities of the surface modes which should show dipole activity.

For the on-top configuration only z displacements need to be considered in the dynamical matrix since both x and y displacements are decoupled. The surface matrices for the on-top site are then given by

$$d(0,0)=\begin{bmatrix}\phi_0''/\Omega_b^2 M_A & 0\\ 0 & 0\end{bmatrix}, \tag{17a}$$

$$d(0,1)=\begin{bmatrix}-\phi_0''/\Omega_b^2 (M_A M_S)^{1/2} & 0\\ 0 & 0\end{bmatrix}, \tag{17b}$$

$$\Delta d(1,1)=\begin{bmatrix}\phi_0''/\Omega_b^2 M_S & 0\\ 0 & 0\end{bmatrix}. \tag{17c}$$

The density of states for the on-top configuration is projected on the relative-normal displacements of the nitrogen and bonding substrate atom as

$$\sum_{L_z,k} \xi_\lambda(L_z,k)\cdot \mathbf{V}^*(L_z,k) = \left[\frac{\xi_{\lambda,z}(0,1)}{M_A^{1/2}}-\frac{\xi_{\lambda,z}(1,1)}{M_S^{1/2}}\right] \Big/ \left[\frac{1}{M_A}+\frac{1}{M_S}\right]^{1/2}, \tag{18}$$

and is shown in Fig. 5(b). From the calculated density of states it is observed that both the $S_1(\bar{X})$ and the $\bar{\Gamma}$ surface resonance are not observed with any appreciable intensity even though they are symmetry allowed to be dipole active. A small contribution from bulk states is observed around 31 meV. The small contribution from the $S_1(\bar{X})$ surface phonon and the $\bar{\Gamma}$ surface resonance results from the fact that the dipole projection for the terminally bonded N_2 is along the bond-stretch displacement. This gives a lower intensity for the surface vibrations for the reasons discussed previously for the short-bridge adsorption site. The lack of any sharp features within the bulk-phonon band in the measured vibrational spectrum for the $(2\times1)N_2$ overlayer is thus consistent with an on-top configuration as seen in the calculated density of states. This conclusion is in agreement with the configuration as deduced empirically from the value of the N-N stretching vibration.

C. (2×1)CO-Cu(110)

The adsorption of CO on Cu(110) possesses many similarities with the adsorption of N_2 on the Ni(110) surface. These similarities have been noticed in previous studies[35,36] where CO also forms a (2×1) ordered phase at $\Theta=0.5$ ML and a compressed incommensurate phase at higher coverages.[40] Similarly, there is only one main CO vibrational band at 2088 cm^{-1} which shifts ~6 cm^{-1} with increased coverage as observed by ir spectroscopy.[41] A second weaker CO vibrational mode was observed at 2104 cm^{-1} at low coverages and has been attributed to CO adsorbed in defect sites.[42]

The similarities between the N_2/Ni(110) and CO/Cu(110) systems allow the previous results for the $(2\times1)N_2$ system to be applied to the (2×1)CO/Cu(110) system by scaling the phonon frequencies occurring within the bulk-phonon bands by 0.8, which is simply the ratio of the maximum bulk-phonon frequencies for Cu and Ni. The measured vibrational spectrum for the (2×1)CO overlayer is shown in Fig. 6. The C-O stretching vibration is observed at 259 meV (2089 cm^{-1}) in agreement with previous ir (Refs. 40 and 41) and EELS (Ref. 43) measurements. Also observed is the C-Cu stretching vibration at 43 meV. We did not observe a band at 85 meV which was reported in the previous EELS study[43] and is most likely due to some impurities since it was only observed at low exposures. As seen in Fig. 6 no spectral features are observed within the bulk-phonon bands, similar to the $(2\times1)N_2$ case. By scaling the Ni results, the $S_7(\bar{X})$ surface phonon should be observed at ~22 meV for CO occupying a short-bridge-site configuration on Cu. Due to the null result and the value of the C-O stretching vibration, an on-top adsorption site can be concluded for the (2×1) overlayer structure.

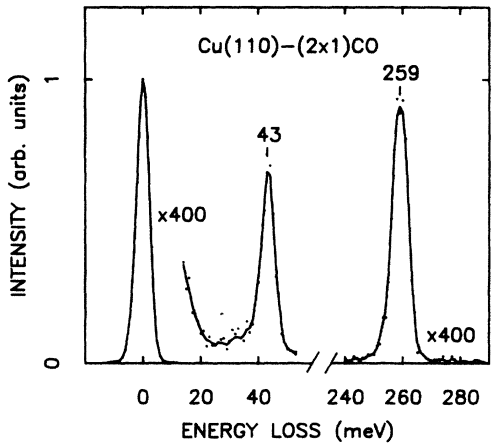

FIG. 6 Electron-energy-loss spectra of Cu(110) with a (2×1)CO overlayer at 80 K.

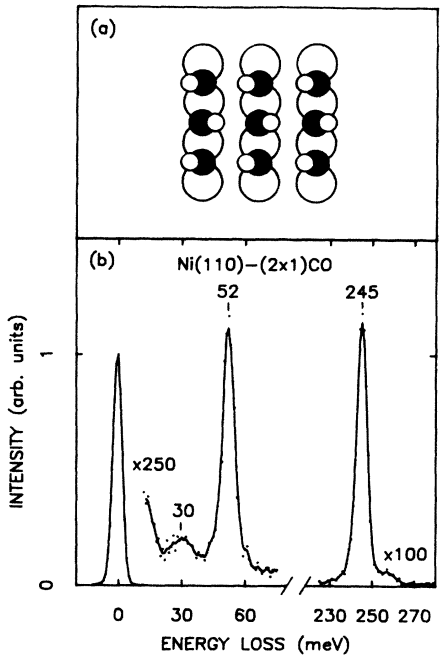

FIG. 7. (a) Schematic model for the Ni(110)-(2×1)CO structure. The smaller solid circles (carbon) and open circles (oxygen) represent the tilted CO molecule. (b) Electron-energy-loss spectra of Ni(110) with a (2×1)CO overlayer at 80 K.

D. (2×1)CO-Ni(110)

The interaction of CO with Ni(110) has been a subject of recent interest due to the different structural configurations which form on this surface depending on the CO coverage.[37] Previous EELS measurements have identified three C-O stretching vibrations corresponding to different adsorption sites.[44,45] Below saturation coverage the two C-O modes, which occur at 242 and 256 meV, have been assigned to short-bridge and on-top adsorption-site configurations, respectively. At saturation coverage corresponding to $\Theta=1$ ML, CO forms an ordered (2×1) overlayer structure. The LEED pattern contains missing $(n/2, 0)$, with n odd, diffraction beams, which indicates a glide-line symmetry along the $[1\bar{1}0]$ direction similar to the previously described hydrogen structure.[45]

The vibrational spectrum for the (2×1)CO overlayer is shown in Fig. 7(b). The C-O and C-Ni stretching vibrations are observed at 245 and 52 meV, respectively, in agreement with previous EELS results.[44] Also observed in Fig. 7(b) is a loss feature within the bulk-phonon bands at 30 meV. Based on LEED and EELS measurements an adsorption-site configuration consisting of alternatively tilted CO molecules in a short-bridge site has been proposed[37] as shown in Fig. 7(a). Recent electron-stimulated desorption ion angular distribution (ESDIAD) measurements have confirmed the tilting of the CO molecule in the (2×1) structure with a tilt angle of 17°–20°.[46] A similar tilted geometry has been determined for the (2×1)CO/Pt(110) structure, although with an on-top adsorption site consistent with the higher CO stretching frequency on that surface.[47]

The symmetry analysis presented for the (2×1)H system can be applied to the adsorption-site configuration in Fig. 7(a) due to the similar point-group symmetry. As was found for the hydrogen case, displacement fields corresponding to the surface modes at the $\bar{X}$ point shown in Fig. 3 are symmetry forbidden to be dipole active, whereas the resonance mode at the $\bar{\Gamma}$ point is symmetry allowed. Furthermore, two vibrational modes corresponding to the frustrated rotational and translational modes of the molecule will be dipole active due to the lower symmetry of the tilted molecule. Based on cluster calculations,[48] the frequency of the frustrated translation is expected to be very low, <10 meV, since to first order this mode does not involve any straining of the nearest-neighbor bonds. The frustrated rotation should be in the frequency range of the metal-carbon vibration.

Lattice-dynamical calculations for 1 ML of untilted CO molecules on the Ni(110) surface show a negligible intensity of the $\bar{\Gamma}$ resonance, similar to the effect observed for the terminally bonded $(2\times1)N_2$ in Fig. 5(b). Further, the inherent dipole activity of this surface resonance is much weaker than the dipole activity of the frustrated translation of N_2 against the surface as evidenced by Figs. 4(b) and 5(c). This leaves the assignment of the 30-meV loss feature in Fig. 7(b) to be due to the frustrated rotational mode of the tilted CO molecule. Similar dipole-active losses have been observed and assigned to frustrated rotations for tilted CO molecules on other transition-metal surfaces.[49] The proposed short-bridge-site geometry in Fig. 7(a) is also consistent with the value of the C-O stretching vibration observed at 245 meV. For a tilted on-top adsorption-site configuration, an additional mode corresponding to the $S_2(\bar{X})$ surface phonon is symmetry allowed to be dipole active. The lack of any additional features at ~18 meV expected for the $S_2(\bar{X})$ surface phonon thus lends additional support for the short-bridge-site configuration shown in Fig. 7(a).

E. (2×1)O-Ni(110) and Cu(110)

The interaction of oxygen with the Ni(110) and Cu(110) surfaces has been the subject of many recent structural in-

vestigations. Considerable interest has been attached to the (2×1) structure which forms on both these surfaces and shows an oxygen-induced reconstruction of the surface layer. For the Cu surface, low-energy ion scattering[50] and He diffraction[51] have concluded a missing-row model for the surface reconstruction where every [001] row is absent. The Ni(110) surface has received considerably more attention with conflicting views on the particular model for the surface reconstruction. Two of the most favored models for the Ni reconstruction are the missing-row (MR) model[52–55] and the sawtooth (SW) model,[56,57] which are shown in Fig. 8. The two models differ by an additional missing row in the second layer for the SW model. It would be expected that the surface vibrational modes would be very sensitive to such a loss of coordination of the surface atoms and can therefore serve as a means of distinguishing between different models of the surface reconstruction.

In the present paper we present results from EELS for the (2×1) reconstruction on both the Cu(110) and Ni(110) surfaces. The surface modes appearing within the bulk-phonon bands are expected to be sensitive to the particular reconstruction, reflecting the additional loss of coordination of the surface atoms in the reconstructed geometry. Lattice-dynamical calculations are shown for the two different models of the reconstruction for Ni(110). The results for Cu can be obtained by simply scaling the results by the ratio of the maximum bulk-phonon frequencies.

The energy-loss spectrum for the (2×1)O surfaces are shown in Fig. 9. Nearly identical oxygen-metal stretching vibrations are observed at 48 and 49 meV on the Cu and Ni surfaces, respectively. These values are in agreement with previous EELS measurements on these surfaces.[55,58] Additional sharp losses are observed below the maximum bulk-phonon frequency at 15 and 30 meV for Ni and 24.5 meV for Cu. Both energy-loss and gain peaks are observed with an intensity ratio which is determined by the Bose-Einstein distribution factor and the crystal temperature. In comparing the EELS spectra on the two surfaces, it is observed that the ratio of the 30- to the 24.5-meV loss scales as the ratio of the maximum bulk-phonon frequencies. This suggests the possibility that these vibrations are related to the motion of the metal substrate atoms and that the reconstruction is similar on both surfaces. The 15-meV loss observed on the Ni surface would then be shifted down to ~12 meV on the Cu surface where it would not be resolvable from the elastic beam.

In calculating the density of states for the dipole-active losses, we use the structural models shown in Fig. 8. The position of the oxygen atom has been determined for the Ni(110) surface by ion-scattering[54,58] and helium-diffraction[53] measurements to be in the long-bridge site 0.25 Å above the center of the topmost nickel rows. With this geometry the O—Ni bond distances are 1.77 and 1.95 Å for the first- and second-layer Ni atoms, respectively. The O-Ni force constant with the second-layer Ni atoms would be expected to be comparable to that for the first-layer Ni atoms due to the similar bond distances. To minimize the number of parameters in the calculation the O-Ni force constants are taken to be the same for the first- and second-layer Ni atoms; the value of the force constant is then uniquely determined by fitting to the measured O-Ni vibrational frequency at 49 meV. Similar to the previous calculations, the Ni-Ni force constants in

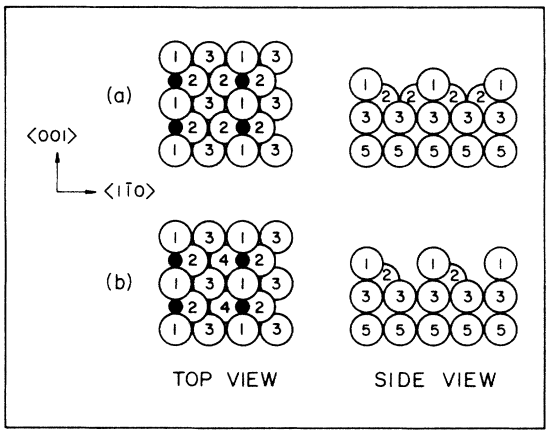

FIG. 8. Models of the (2×1) reconstructed (110) surfaces formed by oxygen adsorption. (a) Missing-row model. (b) Sawtooth model. The small solid circles represent oxygen atoms. The numbers denote sequential layers of the substrate with number 1 corresponding to the surface layer. For each model both the top and side views are shown.

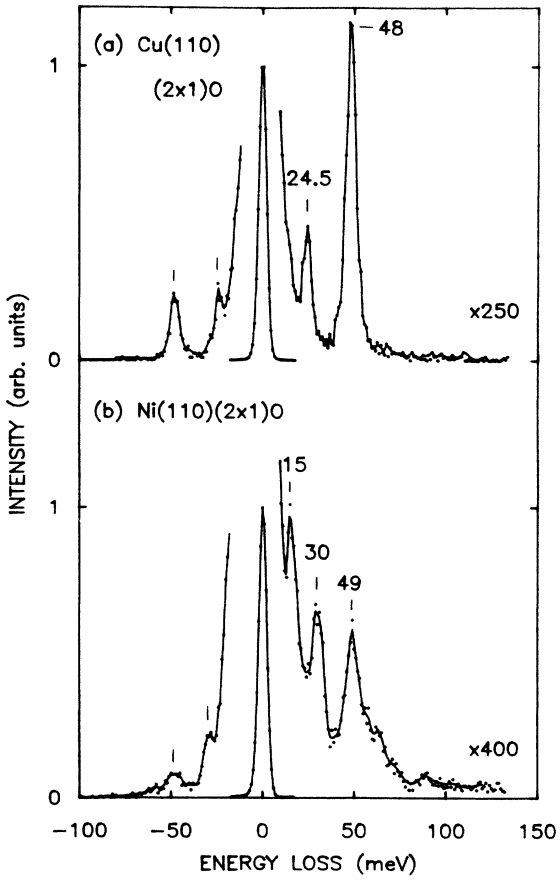

FIG. 9. Electron-energy-loss spectra of (2×1) oxygen overlayers on Cu(110) and Ni(110) at 300 K.

the surface region are taken to be equal to their bulk value.

The calculated density of states are shown in Fig. 10(a) for the MR model of the bare Ni surface. Included in the results for the bare surface is the sum of the density of states for the totally symmetric displacements with respect to the long-bridge site for the first and second Ni layers. The two higher-energy peaks at 21.3 and 31.7 meV result from a breathing motion in the second layer with a polarization in the x direction. The lower-energy peak at 16.9 meV results from the perpendicular motion of the top-layer Ni atoms.

Shown in Fig. 10(b) is the density of states for the oxygen-covered surface. The projection is taken on the perpendicular motion of the oxygen atom to avoid the complexity in modeling the effective charge field for bonding to both the first- and second-layer Ni atoms. As seen in Fig. 10(b), a sharp feature is observed at 30 meV which is shifted down slightly from 31.7 meV on the bare surface. The remaining sharp structure in the density of states of the bare surface is not seen to be reproduced on the oxygen-covered surface except for a broad feature at 24 meV. In comparing to the measured loss spectrum, the 30-meV loss feature is accounted for in the calculation for the MR model; however, no structure is observed at 15 meV in the calculated density of states to correspond to the observed feature in the measured loss spectrum.

The calculated density of states for the SW model is shown in Fig. 11(a) for the bare surface. The lower symmetry in the SW model increases the number of symmetry-allowed displacement fields. In comparison to the MR model a substantial amount of intensity is distributed to lower energies. This results simply from the fact that the restoring forces for the surface atoms are smaller in this model than for the MR model, resulting from the lower coordination of the surface atoms in the SW model in comparison to the MR model. The results for the oxygen-covered surface are shown in Fig. 11(b) for a projection on the perpendicular motion. Sharp spectral features are observed at 15.4, 25.3, and 27.8 meV. The features at 25.3 and 27.8 meV would not be resolved with the 5-meV experimental resolution and would thus appear as one loss peak at $\sim$27 meV. Also shown in Fig. 11(b) is the projection on the parallel motion of the oxygen atom in the x direction. Due to the loss of the additional second-layer Ni atom, the perpendicular and parallel motions are now coupled as seen in Fig. 11(b).

In comparing to the measured loss spectra, the SW model gives two losses at approximately the correct fre-

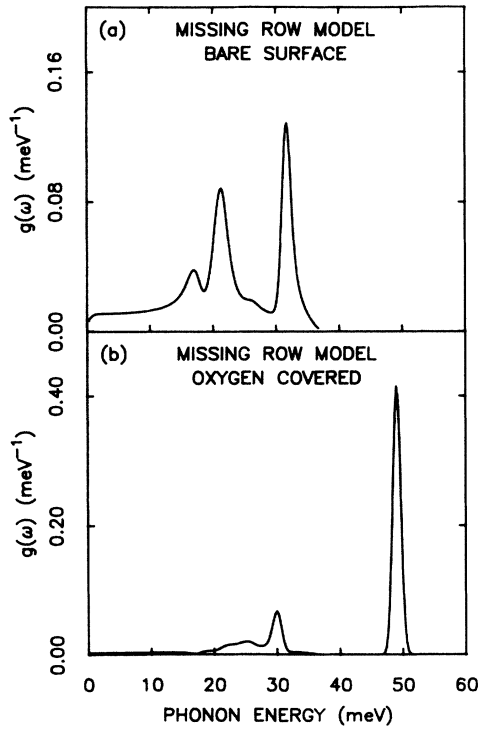

FIG. 10. Results from lattice-dynamical calculations for the missing-row model of the surface reconstruction shown in Fig. 8(a). (a) Summation of the vibrational density of states for projections on the totally symmetric displacements with respect to the long-bridge site, for the first and second layers of the bare Ni surface. (b) Vibrational density of states projected on the perpendicular motion of the oxygen atom in the long-bridge site for the missing-row model. The calculations used a 99-layer slab with a 1.5-meV Gaussian broadening.

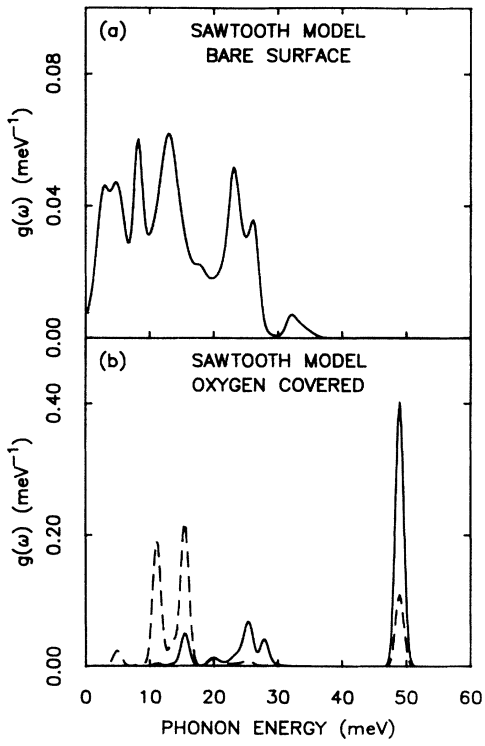

FIG. 11. Results from lattice-dynamical calculations for the sawtooth model of the surface reconstruction shown in Fig. 8(b). (a) Summation of the vibrational density of states for projections on the totally symmetric displacements with respect to the long-bridge site, for the first and second layers of the bare Ni surface. (b) Vibrational density of states projected on the perpendicular (solid line) and parallel (dashed line) motion of the oxygen atom in the long-bridge site of the sawtooth model. The calculations used a 99-layer slab with a 1.5-meV Gaussian broadening.

quencies, which is in better agreement than the MR model. A decisive distinction, however, cannot be made since the agreement with the two models could be made to change by varying the parameters in the calculation. The results do show that the surface modes are extremely sensitive to the coordination of the atoms in the models for the reconstruction and that a larger database obtainable by angular distribution measurements throughout the SBZ, coupled with lattice-dynamical calculations, could contribute to the determination of the structure for the reconstructed surfaces.

VI. CONCLUSION

A variety of adsorbates are observed to form (2×1) superstructures on the fcc (110) surfaces of Ni and Cu. A lattice-dynamical analysis of the energy-loss spectra of these adsorbate structures was achieved using a simple finite-slab method, together with the symmetry selection rules which are operative in dipole scattering. For the (2×1)H structure on Ni(110) the observation of a single resonance mode at 24 meV was found to be in agreement with the buckled-bridge geometry as deduced from He-diffraction and LEED measurements. Based on a comparison of the loss spectra with spectral-density calculations, a terminally bonded configuration was deduced for the (2×1)N_2 and CO structures on the Ni and Cu surfaces, respectively. For the (2×1)CO structure on Ni(110), a loss feature was observed at 30 meV which is assigned to the CO frustrated rotational mode for the proposed structure consisting of alternating tilted CO molecules in the short-bridge site. In the case of oxygen adsorption on these surfaces a reconstruction of the surfaces takes place. The vibrational density of states of the reconstructed surface was calculated for the missing-row and sawtooth models. For the sawtooth model a significant amount of intensity is redistributed to low energies due to the lower coordination of the surface atoms. A comparison of the measured loss spectra with the density of states for the oxygen-covered surfaces favors the sawtooth model for the surface reconstruction. However, a firm distinction between the two models requires a larger database from measurements throughout the surface Brillouin zone. Detailed mapping of the vibrational energy dispersions and the observation of vibrational modes parallel to the surface from off-specular measurements can give further support to the deduced bonding sites.

ACKNOWLEDGMENTS

Support of this research by the U.S. Office of Naval Research under Contracts No. N00014-81-K-0505 and No. N00014-82-K-0576 and the Swedish Natural Science Research Council is gratefully acknowledged.

*Permanent address: Institute of Theoretical Physics, Chalmers University of Technology, S-412 96 Göteborg, Sweden.

[1]H. Ibach and D. L. Mills, *Electron Energy Loss Spectroscopy and Surface Vibrations* (Academic, New York, 1982),

[2]S. Lehwald, J. M. Szeftel, H. Ibach, T. S. Rahman, and D. L. Mills, Phys. Rev. Lett. **50**, 518 (1983); Mu-Liang Zu, B. M. Hall, S. Y. Tong, M. Rocca, H. Ibach, S. Lehwald, and J. E. Black, *ibid.* **54**, 1171 (1985).

[3]S. Anderson, B. J. Persson, M. Persson, and N. D. Lang, Phys. Rev. Lett. **52**, 2073 (1984).

[4]J. M. Szeftel, S. Lehwald, H. Ibach, T. S. Rahman, J. E. Black, and D. L. Mills, Phys. Rev. Lett. **51**, 268 (1983); T. S. Rahman, D. L. Mills, J. E. Black, J. M. Szeftel, S. Lehwald, and H. Ibach, Phys. Rev. B **35**, 589 (1984).

[5]S. Andersson and M. Persson, Phys. Rev. B **24**, 3659 (1981).

[6]R. L. Strong and J. L. Erskine, Phys. Rev. Lett. **54**, 346 (1985).

[7]H. Ibach and D. Bruchman, Phys. Rev. Lett. **44**, 36 (1980).

[8]S. Andersson and B. N. J. Persson, Phys. Rev. Lett. **45**, 1421 (1980).

[9]T. S. Rahman, D. L. Mills, and J. E. Black, Phys. Rev. B **27**, 4059 (1983); J. E. Black, T. S. Rahman, and D. L. Mills, *ibid.* **27**, 4072 (1983); T. S. Rahman, J. E. Black, and D. L. Mills, Phys. Rev. Lett. **46**, 1469 (1981).

[10]M. Persson, Phys. Scr. **29**, 181 (1984).

[11]J. E. Black, in *Vibrations at Surfaces*, edited by R. Caudano, J.-M. Gilles, and A. A. Lucas (Plenum, New York, 1982), p. 57.

[12]G. Allan and J. Lopez, Surf. Sci. **95**, 214 (1980).

[13]V. Bortolani, A. Francchini, F. Nizzoli, and G. Santoro, Solid State Commun. **41**, 369 (1982).

[14]R. L. Strong, B. Firey, F. W. de Wette, and J. L. Erskine, Phys. Rev. B **26**, 3483 (1982); R. L. Strong and J. L. Erskine, *ibid.* **31**, 6305 (1985); Phys. Rev. Lett. **54**, 346 (1985).

[15]M. Persson and S. Andersson, Surf. Sci. **117**, 352 (1982).

[16]M. Persson, J. A. Stroscio, and W. Ho, Phys. Rev. B (to be published).

[17]J. A. Stroscio, M. Persson, S. R. Bare, and W. Ho, Phys. Rev. Lett. **54**, 1428 (1985).

[18]J. A. Stroscio, S. R. Bare, and W. Ho, Surf. Sci. **148**, 499 (1984).

[19]J. A. Stroscio and W. Ho, Rev. Sci. Instrum. (to be published).

[20]J. A. Stroscio and W. Ho, Rev. Sci. Instrum. **55**, 1672 (1984).

[21]W. Ho, R. F. Willis, and E. W. Plummer, Phys. Rev. Lett. **40**, 1463 (1978); Phys. Rev. B **21**, 4202 (1980).

[22]A. A. Lucas and M. Sunjic, Prog. Surf. Sci. **2**, 2 (1972); E. Evans and D. L. Mills, Phys. Rev. B **5**, 4126 (1972); D. M. Newns, Phys. Lett. **60A**, 461 (1977); F. Delanaye, A. Lucas, and G. D. Mehan, Surf. Sci. **70**, 629 (1978); B. N. J. Persson, Solid State Commun. **24**, 573 (1977); D. Sokcevic, Z. Lenac, R. Brako, and M. Sunjic, Z. Phys. B **28**, 677 (1977); B. N. J. Persson, Surf. Sci. **92**, 265 (1980); W. L. Schaich, Phys. Rev. B **24**, 686 (1981); W. L. Schaich, Surf. Sci. **122**, 175 (1982); B. N. J. Persson and J. E. Demuth, Phys. Rev. B **30**, 5968 (1984).

[23]D. L. Mills, Surf. Sci. **48**, 59 (1975).

[24]A. A. Maradudin, R. F. Wallis, and L. Dobrzynski, *Handbook of Surfaces and Interfaces*, (Garland STPM, New York, 1980), Vol. III.

[25]A. A. Maradudin, E. W. Montroll, G. H. Weiss, and I. P. Ipatora, *Lattice Dynamics in the Harmonic Approximation*, 2nd ed. (Academic, New York, 1981).

[26]M. Persson, S. Andersson, and P. A. Karlsson, Chem. Phys.

Lett. **111**, 597 (1984).
[27]R. J. Birgenau, J. Cordes, G. Dolling, and A. D. B. Woods, Phys. Rev. **136**, A1359 (1964); E. C. Svensson, B. N. Brockhouse, and J. M. Rowe, *ibid.* **155**, 619 (1967).
[28]J. E. Black, D. A. Campbell, and R. F. Wallis, Surf. Sci. **115**, 161 (1982).
[29]R. E. Allen, G. P. Alldredge, and F. W. de Wette, Phys. Rev. B **4**, 1661 (1971).
[30]V. Penka, K. Christsmann, and G. Ertl, Surf. Sci. **136**, 307 (1984).
[31]K. H. Rieder and T. Engel, Phys. Rev. Lett. **43**, 373 (1979); **48**, 824 (1980); T. Engel and K. H. Rieder, Surf. Sci. **109**, 140 (1981).
[32]M. Nishijima, M. Jo, and M. Onchi, Surf. Sci. **151**, L179 (1985); N. J. DiNardo and E. W. Plummer, *ibid.* **150**, 89 (1985); L. Olle and A. M. Baro, *ibid.* **137**, 607 (1984); M. Nishijima, S. Masuda, M. Jo, and M. Onchi, J. Electron Spectrosc. Relat. Phenomen. **29**, 273 (1983).
[33]T. H. Upton and W. A. Goddard III, Phys. Rev. Lett. **42**, 472 (1979); J. P. Muscat, Surf. Sci. **110**, 85 (1981); P. Nordlander, S. Holloway, and J. K. Norskov, *ibid.* **136**, 59 (1984); M. Sayers, *ibid.* **136**, 582 (1984).
[34]The assignments of these losses have varied; see M. Jo, M. Onchi, and M. Nishijima [Surf. Sci. **154**, 417 (1985)] for a thorough discussion and also Ref. 32 for further details on the possible assignments.
[35]M. Grunze, P. H. Kleban, and W. N. Unertl, Phys. Rev. Lett. **51**, 582 (1983).
[36]B. J. Bandy, N. D. S. Canning, P. Hollins, and J. Pritchard, J. Chem. Soc., Chem. Commun. **1982**, 58.
[37]B. A. Gurney and W. Ho, J. Vac. Sci. Technol. A **3**, 1541 (1985).
[38]K. Horn, J. DiNardo, W. Eberhardt, H. J. Freand, and E. W. Plummer, Surf. Sci. **118**, 465 (1982).
[39]M. Grunze, R. K. Driscoll, G. N. Burland, J. C. L. Cornish, and J. Pritchard, Surf. Sci. **89**, 381 (1979).
[40]K. Horn, M. Hussain, and J. Pritchard, Surf. Sci. **63**, 244 (1977).
[41]D. P. Woodruff, B. E. Hayden, K. Prince, and A. M. Bradshaw, Surf. Sci. **123**, 397 (1982).
[42]P. Hollins, K. J. Davies, and J. Pritchard, Surf. Sci. **138**, 75 (1984).
[43]J. F. Wendelken and M. V. Ulehla, J. Vac. Sci. Technol. **16**, 441 (1979).
[44]M. Nishijima, S. Matsuda, Y. Sakisaka, and M. Onchi, Surf. Sci. **107**, 31 (1981); B. J. Bandy, M. A. Chesters, P. Hollins, J. Pritchard, and N. Shepard, J. Mol. Struct. **80**, 203 (1982).
[45]R. M. Lambert, Surf. Sci. **49**, 325 (1975).
[46]W. Riedl and D. Menzel, in *Proceedings of the Second International Workshop, Desorption Induced by Electronic Transitions (DIET II)*, edited by W. Brenig and D. Menzel (Springer-Verlag, Berlin, 1985).
[47]P. Hoffmann, S. R. Bare, N. V. Richardson, and D. A. King, Solid State Commun. **42**, 654 (1982).
[48]N. V. Richardson and A. M. Bradshaw, Surf. Sci. **88**, 255 (1979).
[49]W. Erley, J. Vac. Sci. Technol. **18**, 472 (1981).
[50]P. N. Bronckers and A. G. J. DeWit, Surf. Sci. **112**, 133 (1981).
[51]J. Lapujoulade, Y. LeCruer, M. Lefort, Y. Lejay, and E. Maurel, Surf. Sci. **118**, 103 (1982).
[52]L. K. Verheij, J. A. Van den Berg, and D. G. Armour, Surf. Sci. **84**, 408 (1979); J. A. Van den Berg, L. K. Verheij, and D. G. Armour, *ibid.* **91**, 218 (1980); R. G. Smeenk, R. M. Tromp, and F. W. Saris, *ibid.* **107**, 429 (1981).
[53]T. Engel, K. H. Rieder, and P. Batra, Surf. Sci. **148**, 321 (1984).
[54]H. Niehus and G. Comsa, Surf. Sci. **151**, L171 (1985).
[55]A. M. Baro and L. Olle, Surf. Sci. **126**, 170 (1983).
[56]M. Schuster and C. Varelas, Surf. Sci. **134**, 195 (1983).
[57]A. M. Baro, G. Binnig, H. Rohrer, Ch. Gerber, E. Stoll, A. Baratoff, and F. Salvan, Phys. Rev. Lett. **52**, 1304 (1984).
[58]J. F. Wendelken, Surf. Sci. **108**, 605 (1981).